applied optics

Thick multilayered (silica/gold) dipole nano-antenna

Abdul Khaleque,[1] Evgeny G. Mironov,[1,2] Liming Liu,[1] and Haroldo T. Hattori[1,*]

[1]School of Engineering and Information Technology, UNSW Australia, Canberra, ACT 2610, Australia
[2]Department of Electronic Materials Engineering, Australian National University, Canberra, ACT 0200, Australia
*Corresponding author: h.hattori@adfa.edu.au

Received 28 July 2015; revised 25 October 2015; accepted 26 October 2015; posted 27 October 2015 (Doc. ID 246917); published 25 November 2015

Nano-antennas are the optical equivalent of antennas that are used to transmit and receive information at radio frequencies. These antennas have been used in different applications in photonics such as optical imaging, particle manipulation, bio-sensing, and improvement of the performance of solar cells. In this article we study composite nano-antennas made of alternating layers of silica and gold. We show that a 50% filling factor leads to a 2.0 times increase in the electric-field enhancement factor when compared with a pure-gold antenna.

OCIS codes: (240.6680) Surface plasmons; (240.3990) Micro-optical devices.

http://dx.doi.org/10.1364/AO.54.010063

1. INTRODUCTION

Nano-antennas are plasmonic devices that are widely used in contemporary photonics research to enhance local photophysical phenomena [1–3]. When an incident wave reaches the antenna, the latter converts it into localized surface plasmons (LSPs) [4]. The subsequent coupling between the excited LSPs leads to a strong confinement of the incoming light (assuming it has the correct polarization). This in turn, results in the enhancement of specific electric-field components, which can be further utilized in different plasmonic applications including trapping of nano-particles [5] and photovoltaics [6].

There are different types of nano-antennas ranging from integrated dipole devices [7,8] and directional Yagi-Uda antennas [9,10] to broadband spiral [11] and Charnia-like structures [12]. In their simplest form antennas are constructed by sandwiching a dielectric media between two metallic regions, which is typically achieved by creating a nano-scale air gap by using electron beam lithography or focused ion beam (FIB) milling. As for choice of utilized materials, most structures are fabricated from metals; however, dielectric [13,14] and semiconductor [15] nano-antennas have also been demonstrated.

One of the trends in recent photonic research is the study of composite structures, for example, hyperbolic metamaterials [16] and multilayered waveguides [17,18]. The combination of different materials within a single structure allows the modification of interaction with the incoming radiation, therefore achieving new optical properties such as high values of effective refractive index [19] or the improvement of the confinement of light [20]. Following a similar approach we introduce bi-material Au/SiO_2 dipole nano-antennas and then numerically study their ability to enhance the incident electric field. More precisely, we show that the Au/SiO_2 material combination is generally preferable and a structure with a filling factor of 50% is capable of generating 2.0 times higher electric fields than that made of pure gold.

2. DESCRIPTION OF THE DEVICE

The considered multilayered structure is schematically shown in Fig. 1(a). It is a typical dipole nano-antenna composed of two equal arms of length L_{arm} and width W_{arm}, separated by an air gap with width W_{gap}. Each arm of the antenna has a thickness of $H_{\mathrm{total}} = 300$ nm and consists of five 60 nm thick bi-composite layers, which, in turn, are formed by a combination of gold (thickness H_{Au}) and SiO_2 (thickness H_{sio2}) as outlined in Fig. 1(a) above. The filling factor of gold is given by a parameter G:

$$G = \frac{H_{\mathrm{Au}}}{H_{\mathrm{Au}} + H_{\mathrm{SiO2}}}, \tag{1}$$

which changes from 0 (only SiO_2) to 1 (pure Au device). The whole antenna is placed on top of a semi-infinite SiO_2 substrate and is surrounded by air.

The dipole nano-antenna is numerically analyzed by using commercial finite-difference time-domain software *RSOFT FULLWAVE* [21]. The structure is designed to operate at the free-space wavelength (λ) of 1053 nm. The incoming light is incident normally to the structure with the main electric field along the x-direction [see Fig. 1(b) for details]. The vertical grid

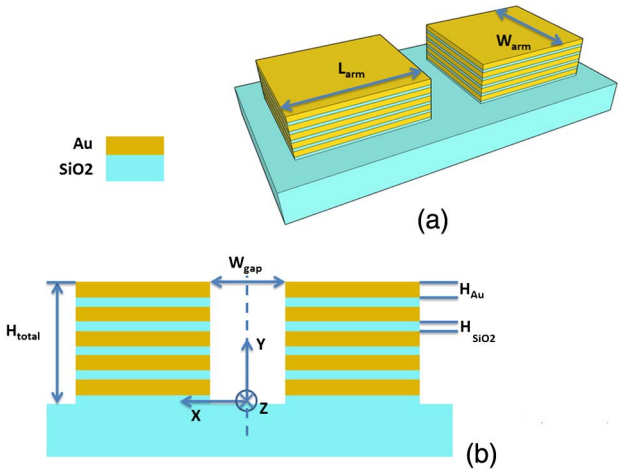

Fig. 1. (a) Multilayered dipole nano-antenna. (b) Transversal view of the antenna.

size Δy is chosen as 5 nm, while $\Delta z = 10$ nm and $\Delta x \leq W_{gap}/5$. The grid sizes for the metallic regions are chosen as $\Delta x = \Delta y = \Delta z = 3$ nm and the time step is set to 8×10^{-18} s. The whole simulation area is terminated by perfectly matching layers. SiO_2 and air are modelled as $n_{SiO2} = 1.45$ and $n_{air} = 1$, respectively. The refractive index of gold is calculated according to the software's dispersive model [21]:

$$\varepsilon(\omega_{\text{Fullwave}}) = 1 + \sum_{k}^{6} \frac{\Delta\varepsilon_k}{-a_k(\omega_{\text{FullWAVE}})^2 - b_k(i\omega_{\text{FullWAVE}}) + c_k}, \tag{2}$$

where ω_{FullWAVE} denotes FullWAVE's computational frequency (which is the angular frequency normalized on the speed of light in vacuum: $\omega_{\text{FullWAVE}} = \omega_0/c_{vac}$; $c_{vac} = 3 \times 10^{14}$ μm/s); and a, b, c, and $\Delta\varepsilon$ are the numerical coefficients summarized in Table 1.

Since the dimensions of the individual metal/dielectric layers are significantly smaller than the wavelength of interest, the whole antenna arm could be treated as having an effective permittivity, ε_{eff}, which is calculated according to the Maxwell–Garnett theory [22] as

$$\varepsilon_{\text{eff}} = \frac{\varepsilon_1\varepsilon_2}{G\varepsilon_2 + (1-G)\varepsilon_1}, \tag{3}$$

where ε_1 and ε_2 denote the permittivities of two media (either Au or SiO_2). In numerical simulations the considered layers are always modelled explicitly, and, thus, the wave propagation is further calculated without implementing the effective medium approach. However, the latter description proves to be useful for the interpretation of obtained results, and, for this reason, ε_{eff} is found for gold/silicon dioxide cases as shown in Fig. 2(a).

Table 1. Dispersion Coefficients from the Material Library [21]

Gold			
$\Delta\varepsilon$	a	b	c
1589.516	1	0.268419	0
50.19525	1	1.220548	4.417455
20.91469	1	1.747258	17.66982
148.4943	1	4.406129	226.0978
1256.973	1	12.63	475.1387
9169	1	11.21284	4550.765

In this article the magnitude of the relative electric field at a given position (x, y, z), i.e., $F_{\text{rel}}(x, y, z)$, is defined as

$$F_{\text{rel}}(x, y, z) = \left| \frac{E_x(x, y, z)}{E_{x,\text{inc}}} \right|, \tag{4}$$

where $|E_x(x, y, z)|$ is the magnitude of the electric field at a position (x, y, z) and $|E_{x,\text{inc}}|$ is the magnitude of the incident electric field. It is assumed that the source is a Gaussian wave with a very large spot-size diameter (spot-size diameter of 20 μm), much larger than the nano-antenna. The antenna is placed between $-L_{\text{arm}} - W_{\text{gap}}/2 < x < L_{\text{arm}} + W_{\text{gap}}/2$, $-W_{\text{arm}}/2 < z < W_{\text{arm}}/2$, and $0 < y < h_{\text{total}}$ as illustrated in Fig. 1(b). Since this factor strongly depends on the y position where the electric field is being measured and does not significantly change with the coordinates x and z inside the antenna, the average electric-field enhancement factor is defined as

$$F_{average} \frac{\int_0^{H_{total}} F_{rel}(x = 0, y, z = 0)dy}{H_{total}} \tag{5}$$

Typically, F_{average} can reach the values above 7.5 [1,8] making such antennas suitable for many applications including nanoparticle detection, nano-imaging, and surface enhanced. Raman scattering. plots showing variations with x and z are later included in the text and do not have significant variations in the regions farther away from the composite gold/silica regions.

3. NUMERICAL ANALYSIS OF THE NANO-ANTENNAS

Initially, the width of the gap (W_{gap}) is assumed to be 60 nm. This is a reasonable gap width that could eventually be fabricated by using FIB milling or electron-beam lithography systems. As previously mentioned, the total height of the antenna is assumed to be $H_{\text{total}} = 300$ nm. As a frame of reference, let us consider the cases of pure gold ($G = 1.0$) and pure silica ($G = 0$). After optimizing the dimensions of the antenna to operate at 1053 nm, we obtain $W_{\text{arm}} = 75$ nm and $L_{\text{arm}} = 150$ nm. F_{average} for pure gold is quite flat for wavelengths between 900 and 1100 nm (close to 4.6), while it is almost constant for pure silica (around 1.6) as can be observed in Fig. 2(b).

The electric-field distributions along the vertical direction for this thick antenna for $G = 0$ and $G = 1$ at $(x = 0, z = 0)$ are shown in Fig. 3. The field does not change significantly in pure silica although it is a bit stronger at mid-height; however, in pure gold the field is significantly stronger closer to the silica substrate. It reaches a maximum at about 50 nm and then decays as it approaches the upper-air boundary at $y = 300$ nm.

The next step is to create nano-antennas based on interleaved layers of gold and silica. The structures are re-designed to maximize the average electric-field enhancement factor at 1053 nm, for example, when $G = 0.5L_{\text{arm}}$ is changed from 150 nm to the optimized value of $L_{\text{arm}} = 175$ nm. The spectra

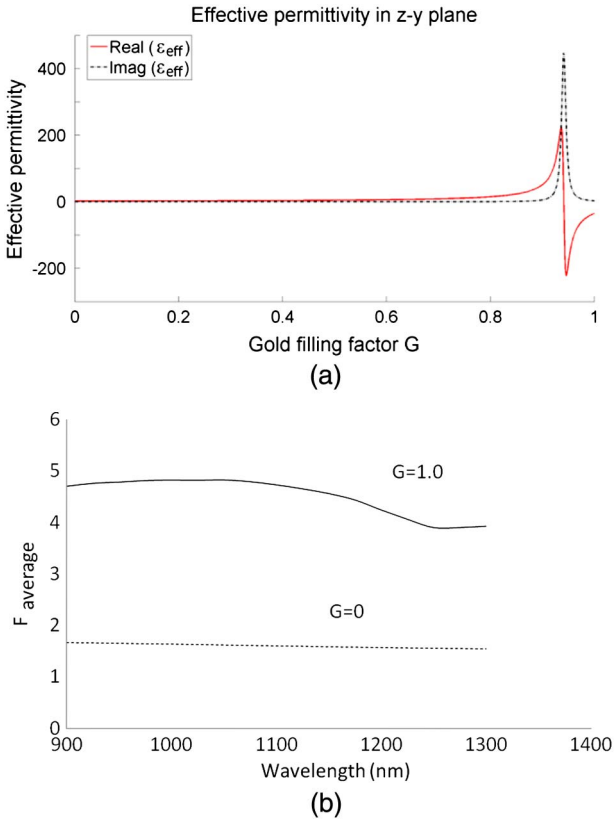

Fig. 2. (a) ε_{eff} of multi-layered structures in y–z plane and (b) F_{average} as a function of frequency for pure gold (solid curve) and pure silica (dotted curve).

of the optimized antennas for different filling factors are shown in Fig. 4. The highest value of F_{average} is obtained for $G = 0.5$ with a maximum value of $F_{\text{average}} = 8.93$. Also, the spectrum for $G = 0.5$ is broader than the spectra for other values of G. Figure 2(a) shows the effective index of the multilayered structure according to the Maxwell–Garnett theory. The effective index for $G = 0.5$ at 1053 nm is about $\varepsilon_{\text{eff}} = 4.81 - j0.0274$. One potential explanation for the larger F_{average} at $\lambda = 1053$ nm for a 50% filling factor is that the silica layers reduce the ohmic losses of the combined gold-silica

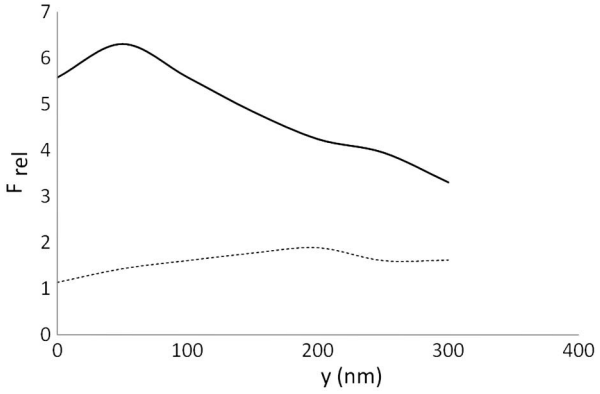

Fig. 3. F_{rel} along the vertical direction at $(x = 0, z = 0)$ for pure gold (solid curve) and pure silica (dotted curve).

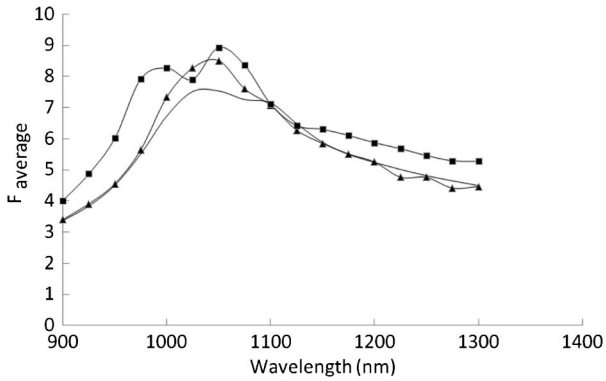

Fig. 4. F_{average} for $G = 0.25$ (solid curve), $G = 0.5$ (solid curve with square markers), and $G = 0.75$ (solid curve with triangular markers).

antenna. In fact many modern-day power electric transformers are based on multi-layered magnetic-dielectric structures to reduce the loss in the magnetic core of the transformers.

The relative electric-field distribution for $G = 0.5$ is shown in Figs. 5(a) and 5(b). The electric field is highest along the plane $y = 150$ nm. For example, along the line $(x = 0, z = 0)$, the electric-field enhancement at $(x = 0, y = 150$ nm, $z = 0)$ is 14.2 while the electric-field enhancement factors close to the silica substrate and air boundary are 3.04 and 9.27, respectively. A change in the position of the maximum electric field can be explained by the interference of the waves inside the multi-layered structure. The electric-field profile at $y = 150$ nm is shown in Fig. 5(b). Along the z-direction it is nearly uniform but weakens on the border of the nano-antenna and air. On the border of the antenna the electric field diffracts and drops by 20%. Along the x-direction there is an increase in the field close to the boundary between the air gap (it reaches a maximum value of 16.21) and then drops considerably at the edges of the multi-layered structure by more than 50%. Based on Figs. 5(a) and 5(b) it seems that the variations in the electric field are much stronger in the y-direction.

While the maximum electric field is located at mid-height when $G = 0.5$, it changes its location as the filling factor is varied as can be observed in Fig. 6. For $G = 0.75$ it is located closer to the silica substrate and for $G = 0.25$ it is located closer to the air boundary. The position of the maximum electric field is a result of the multi-scattering of light inside the composite nano-antenna and depends on the thickness of the individual layers and the total thickness of the nano-antenna. However, in this particular nano-antenna it seems that the higher the G is the closer the peak is to the substrate.

So far, the width of the gap has been kept constant. If the dimensions of the air gap are changed the coupling between the arms of the antenna will change, and consequently, the resonance wavelength of the antenna. For example, the optimized dimensions for $W_{\text{gap}} = 30$ nm are $L_{\text{arm}} = 165$ nm and $W_{\text{arm}} = 80$ nm (strong coupling between the arms) while the optimized dimensions for $W_{\text{gap}} = 120$ nm are $L_{\text{arm}} = 195$ nm and $W_{\text{arm}} = 95$ nm (weak coupling between the arms). After optimizing all dimensions of the antenna while keeping its thickness as $H_{\text{total}} = 300$ nm and $G = 0.5$, the

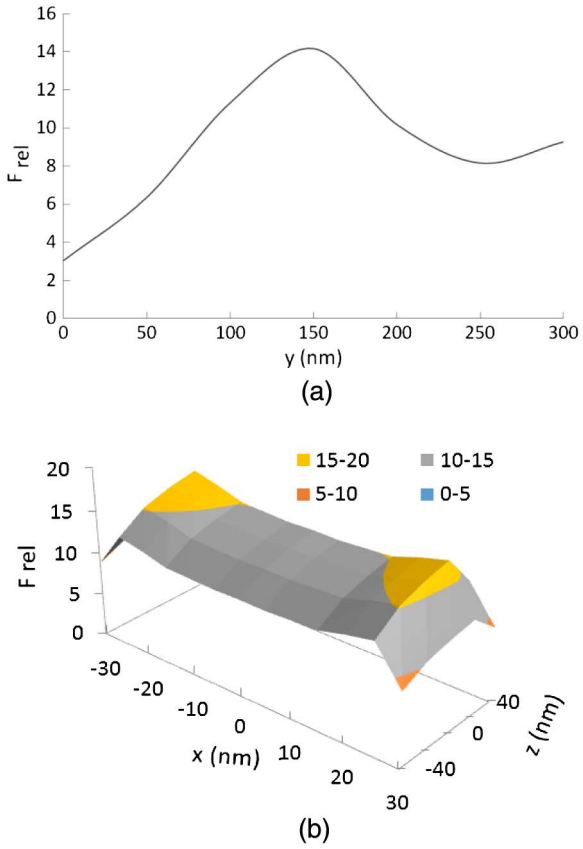

Fig. 5. Electric-field distribution for $G = 0.5$ and $W_{gap} = 60$ nm. (a) Electric-field distribution (E_x) along the vertical direction at ($x = 0, z = 0$). (b) Electric-field distribution at $y = 150$ nm (middle of the nano-antenna).

curve for $F_{average}$ for different values of W_{gap} is shown in Fig. 7. A nearly exponential dependence of $F_{average}$ with W_{gap} can be observed. $F_{average}$, for $W_{gap} = 120$ nm, is about 5.0.

Figure 8 shows $F_{average}$ as a function of the wavelength for the optimized nano-antenna with $G = 0.5$ and $W_{gap} = 30$ nm. The maximum average electric-field enhancement is about 16.5 at the resonance wavelength of 1053 nm. In comparison with the results for a $W_{gap} = 60$ nm, the average electric-field enhancement factor has nearly doubled.

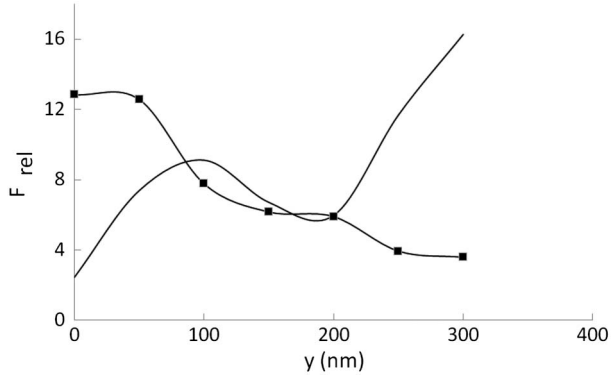

Fig. 6. Electric-field distribution for $W_{gap} = 60$ nm and $G = 0.25$ (solid curve) and $G = 0.75$ (solid curve with square markers).

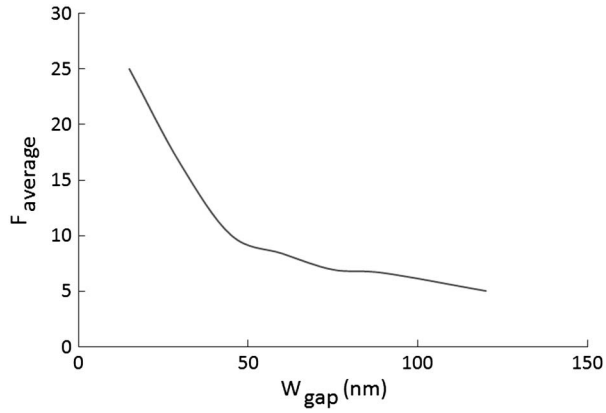

Fig. 7. Electric-field enhancements in monolithic Au nano-antenna ($G = 1$) for different gap widths for a 50% filling factor.

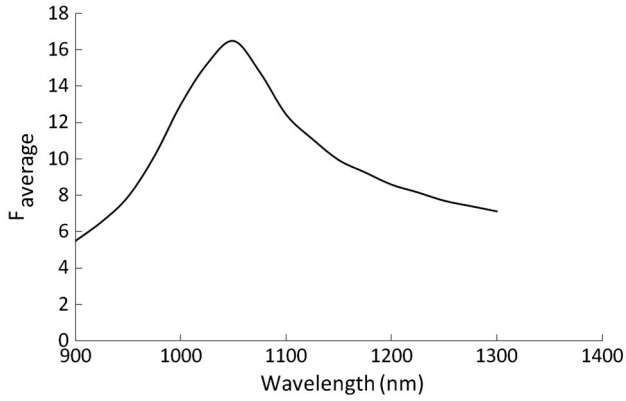

Fig. 8. $F_{average}$ spectrum for $G = 0.5$ and $W_{gap} = 30$ nm.

The electric-field distribution at 1053 nm ($G = 0.5$, $W_{gap} = 30$ nm) is shown in Fig. 9 (solid line). The electric field reaches its peak at the middle of the multi-layered antenna with relative electric-field strength of 26 in the middle of the antenna. The electric field is weaker at the lower boundary of

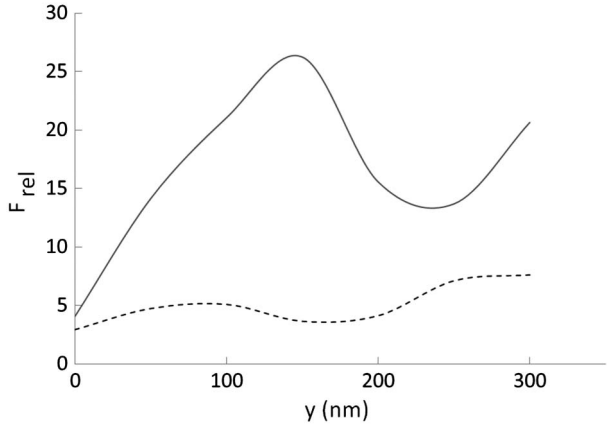

Fig. 9. Relative electric-field strength for $G = 0.5$ and $W_{gap} = 30$ nm (solid line) and $W_{gap} = 120$ nm (dotted line).

the nano-antenna and the silica substrate. Although the maximum value is different, the field profile is somewhat similar to the one for $W_{gap} = 60$ nm.

A different scenario occurs when the gap width is changed to 120 nm as can be observed in Fig. 9 (dotted line). A maximum of the electric field is shifted from 150 to 100 nm while the electric field is stronger at the boundary with air. It seems that the interference of the wave inside the antenna also depends upon the gap width and there is a shift of the maxima of the electric field.

In any case, it seems that a filling factor of 50% leads to the highest average electric-field enhancement, and the introduction of a dielectric has clearly improved the performance of the antenna.

4. CONCLUSIONS

In this work we have numerically studied the electric-field enhancement factors of bi-composite Au/SiO_2 dipole nano-antennas. The initial calculations showed the improved performance of the metal/dielectric design and its performance was further compared with a pure-gold device (which was used as a reference). When the filling factor is set to 50%, the average electric-field enhancement factor is increased by a factor of 2.0 and the electric field is located at mid-height of the antenna.

From a practical point of view, the fabrication of the proposed multilayered nano-antennas is not very complicated and is similar to the case of monolithic ones. Initially, the layers can be deposited on the substrate by means of electron-beam evaporation and/or sputtering, and then the pattern can be milled by using the FIB system.

Funding. Asian Office of Aerospace Research and Development (AOARD FA2386-15-1-4064).

REFERENCES

1. P. Biagioni, J. Huang, and B. Hecht, "Nanoantennas for visible and infrared radiation," Rep. Prog. Phys. **75**, 024402 (2012).
2. E. S. Ünlü, R. U. Tok, and K. Şendur, "Broadband plasmonic nano-antenna with an adjustable spectral response," Opt. Express **19**, 1000–1006 (2011).
3. N. Berkovitch, P. Ginzburg, and M. Orenstein, "Nano-plasmonic antennas in the near infrared regime," J. Phys. **24**, 073202 (2012).
4. S. V. Boriskina and L. D. Negro, "Multiple-wavelength plasmonic nanoantennas," Opt. Lett. **35**, 538–540 (2010).
5. W. Zhang, L. Huang, C. Santschi, and O. J. F. Martin, "Trapping and sensing 10 nm metal nanoparticles using plasmonic dipole antennas," Nano Lett. **10**, 1006–1011 (2010).
6. P. Bharadwaj, B. Deutsch, and L. Novotny, "Optical antennas," Adv. Opt. Photon. **1**, 438–483 (2009).
7. F. González and G. Boreman, "Comparison of dipole, bowtie, spiral and log-period IR antennas," Infrared Phys. Technol. **46**, 418–428 (2005).
8. E. G. Mironov, Z. Li, H. T. Hattori, K. Vora, H. H. Tan, and C. Jagadish, "Titanium nano-antenna for high-power pulsed operation," IEEE J. Lightwave Technol. **31**, 2459–2466 (2013).
9. I. S. Maksymov, I. Staude, A. E. Miroshnichenko, and Y. S. Kivshar, "Optical Yagi-Uda nanoantennas," Nanophotonics **1**, 65–81 (2012).
10. E. G. Mironov, A. Khaleque, L. Liu, I. S. Maksymov, and H. T. Hattori, "Enhancing weak optical signals by using a plasmonic Yagi-Uda Nano-antenna array," Photon. Technol. Lett. **26**, 2236–2239 (2014).
11. D. K. Kotter, S. D. Novack, W. D. Slafer, and P. J. Pinhero, "Theory and manufacturing processes of solar nanoantenna electromagnetic collectors," J. Sol. Energy Eng. **132**, 011014 (2010).
12. Z. Li, H. T. Hattori, and E. G. Mironov, "Charnia-like broadband plasmonic nano-antenna," J. Mod. Opt. **60**, 790–796 (2013).
13. A. E. Krasnok, A. E. Miroshnichenko, P. A. Belov, and Y. S. Kivshar, "All-dielectric optical nanoantennas," Opt. Express **20**, 20599–20604 (2012).
14. G. Pellegrini, G. Mattei, and P. Mazzoldi, "Light extraction with dielectric nanoantenna arrays," ACS Nano **3**, 2715–2721 (2009).
15. S. Law, L. Yu, A. Rosenberg, and D. Wasserman, "All-semiconductor plasmonic nanoantennas for infrared sensing," Nano Lett. **13**, 4569–4574 (2013).
16. I. V. Iorsh, I. S. Mukhin, I. V. Shadrivov, P. A. Belov, and Y. S. Kivshar, "Hyperbolic metamaterials based on multilayer graphene structures," Phys. Rev. B **87**, 075416 (2013); Erratum 88, 039904 (2013)
17. H. Hu, D. Ji, X. Zeng, K. Liu, and Q. Gan, "Rainbow trapping in hyperbolic metamaterial waveguide," Sci. Rep. **3**, 1249 (2013).
18. Y. He, S. He, J. Gao, and X. Yang, "Giant transverse optical forces in nanoscale slot waveguides of hyperbolic metamaterials," Opt. Express **20**, 22372–22382 (2012).
19. Y. He, S. He, J. Gao, and X. Yang, "Nanoscale metamaterial optical waveguides with ultrahigh refractive indices," J. Opt. Soc. Am. B **29**, 2559–2566 (2012).
20. E. G. Mironov, L. Liu, H. T. Hattori, and R. M. De La Rue, "Analysis of silica filled-slot waveguides based on hyperbolic metamaterials," J. Opt. Soc. Am. B **31**, 1822–1828 (2014); Erratum 31, p. 2285 (2014).
21. FullWAVE 8.3," RSoft Design Group, 2011, http://www.rsoftdesign.com.
22. A. Sihvola, *Electromagnetic Mixing Formulas and Applications* (Institution of Electrical Engineering, 1999).